Chapter 5

Results and Discussion

This chapter discusses the results obtained from this work. This include the input channel through interference pattern generated at the waveguide's output, the finding from the simple vision system, procedures on refining channel's position via developing active alignment algorithm and the conclusion of the results for direct UV writing

5.1: Waveguide Alignment

5.1.1: Image Analysis for Waveguide Alignment

This section presents the results obtained from the simple vision system developed for the waveguide alignment with the assistance of a simple jog of stepper motor control. Images with three different resolutions were taken by a USB web-camera for the fiber which is aligned to the input waveguide to determine the respective position of both optical devices. Fig. 5.1 shows the pictures taken at the resolution of 1024x768 during the process of this alignment method.

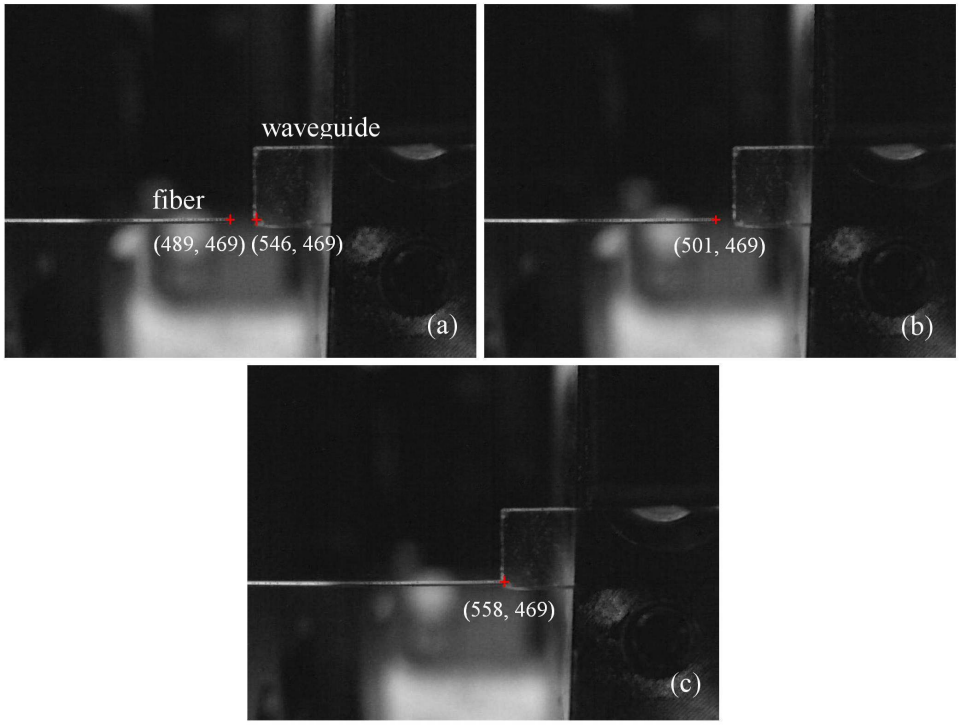

Fig. 5.1: A series of photos captured closely on the aligned waveguides at the resolution of 1024x768

As shown in Fig. 5.1a, the respective position of fiber was recorded at (489, 469) and waveguide was (546, 469). After calibration, movement of 200μm by fiber, the fiber was placed at (501, 469); this resulted the *m* value (from Eqn. 4.1) 16.67μm/pixel and a separation value of 45pixels. Thus the fiber was required to move another 750μm to be in contact with the waveguide's input facet. From Fig. 5.1c, the fiber seems to be in contact with the waveguide's input facet after the 750 μm movement. In fact the fiber had already pushed the waveguide away to a new position at (558, 469). This failure was thought to be related with the insufficient resolution. Therefore the whole procedure was repeated with pictures taken at resolution of 1280x1024, which are shown in Fig. 5.2.

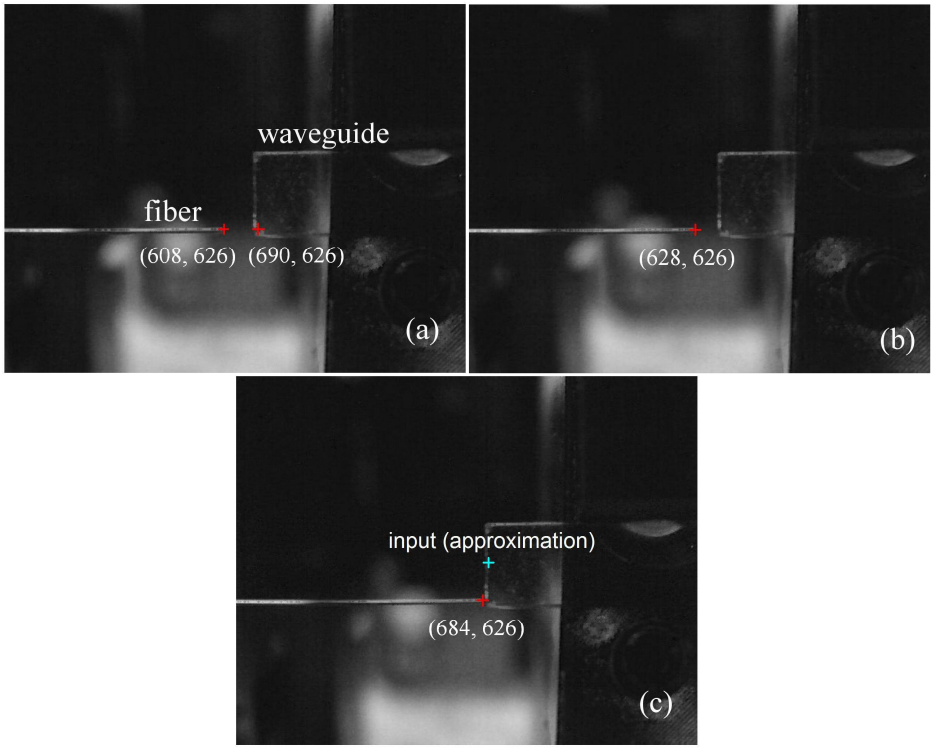

Fig. 5.2: A series of pictures taken on closely aligned waveguide at the resolution of 1280x1024

At this repetition, the initial fiber position was recorded at (608, 626) whereby the position of waveguide was (690, 626). After a constant movement of fiber over a distance of 200µm, fiber was moved to (628, 626) which yielded an *m* value of 10µm/pixel and separation of 45pixels. Therefore, according to Eqn. 4.3, the fiber was moved 620µm towards the waveguide. As shown in Fig. 5.2c, even though after the travel proposed by Eqn. 4.3, there was still a gap of 6pixels for the fiber to be in contact with the waveguide. Despite this, optical signal can still be coupled into the waveguide through that spacing. Hence, fiber is moved to the position in front of the input channel where the position is an approximation. This estimation on input location is made from the assumption that the input channel is fabricated right in the middle of the waveguide's input facet. After the analysis on positions has been done, a series of pictures on waveguide alignment were taken and shown in Fig. 5.3.

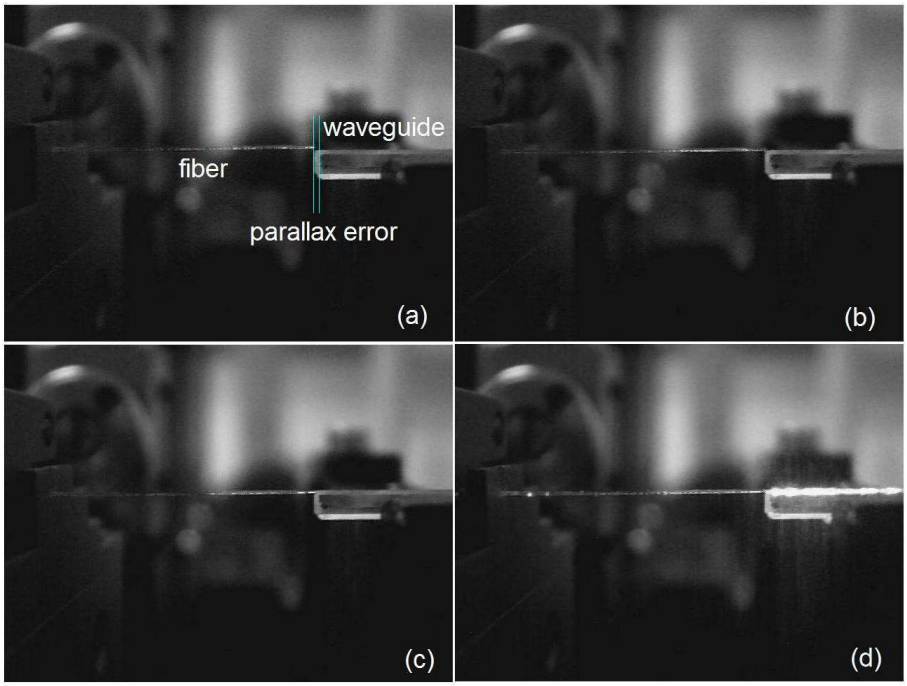

Fig. 5.3: Side view on waveguide alignment

Unfortunately, the fiber was unable to align to the input channel correctly due to the unknown location of input channel, the failed of the assumption. From Fig. 5.3a, parallax error (perspective error) was observed to occur at waveguide's input facet, and the lauch fiber is located within that error region due to the inaccurate information inherited from the parallax error.

Both the attempts failed to satisfactorily align the fiber to waveguide's input due to the imprecise information given by the picture as well as the uncertainty on input waveguide's location. The occurrence of these errors is attributed to several factors. One is the nature of the webcam and the subsequent pixelated information obtained. The webcams being used in this work is not equipped with telecenteric lens, therefore producing images with perspective error. Perspective error is a form of parallax error which originated from the displacement on apparent position of object derived from different lines of sight. Hence, the input face of the waveguide was recorded to have

two different positions. Fig. 5.4 illustrates the perspective error caused by non-telecentric lens.

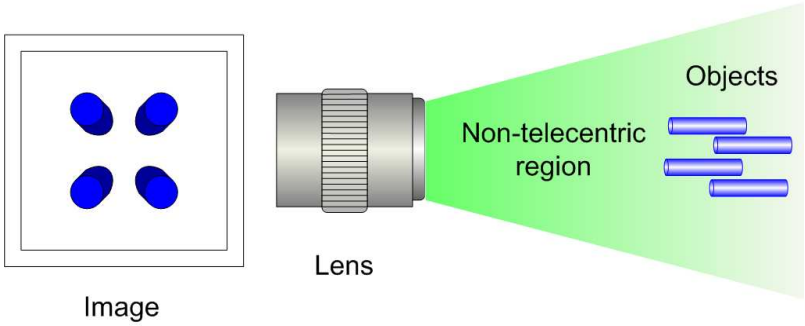

Fig. 5.4: Perspective error caused by a non-telecentric lens [1]

5.1.2: Initial Light Seeking from Interference

As mentioned in previous chapter, this technique is used to perform the initial light seeking task to unveil the location of input channel before fine alignment or pigtailing on waveguides continues. Through the use of this method, input channel was found easily without development of any complicated alignment algorithms. Illustration and part of the results on the search of the initial light from the 1-by-4 optical splitter made of silica on quartz platform is shown in Fig. 5.5a-5.5d.

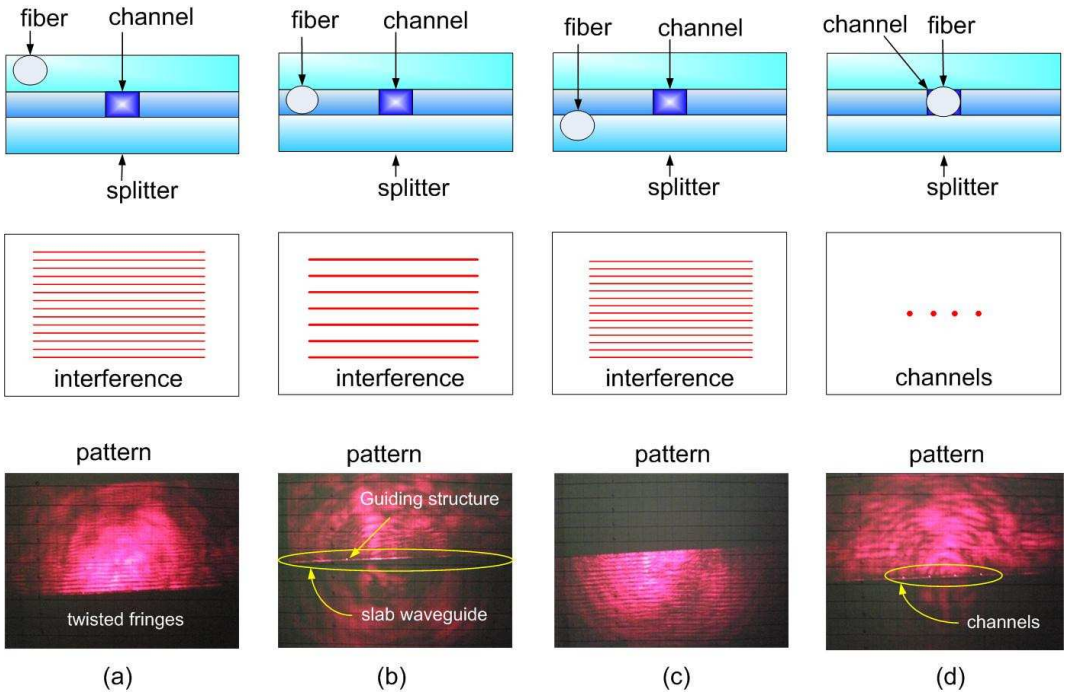

Fig. 5.5a-5.5d (from left to right): Process of first light seeking and the resultant interference pattern

From the attached results on Fig. 5.5a-5.5d, it is clear that interference pattern slowly evolves corresponding to the fiber's movement as mentioned in the last chapter. Fine interference patterns were formed when the fiber was located above the waveguide; and the fringes start to grow in size and in separation when the light source begins to travel downwards into the various glass layers. These changes were apparent and

became distorted when the light source entered a particular region. Within that region, the interference pattern appeared to be twisted (refers to Fig. 5.5) and behaved similar to clouds movement when the light travelled transversely at that region. When light source is moved further down, the twisted pattern is accompanied by a bright fringe which may correspond to the high refractive index core layer. Hence, the region where the interference pattern behaved awkwardly may be the boundary between over-cladding and core layer. With cautious adjustments in the transverse direction of light source relative to input facet, guiding line structure is first spotted and followed by the output channels. Output of guiding line structure within the splitter is shown in a single spot whereas the output channels were represented by 4 bright dots. Judgments on these outcomes are based on the behavior of both occurrences where they were fading off when light source was away, and re-appeared when the light source is moved back to the position. Images of these outcomes are shown in Fig. 5.6a and 5.6b respectively.

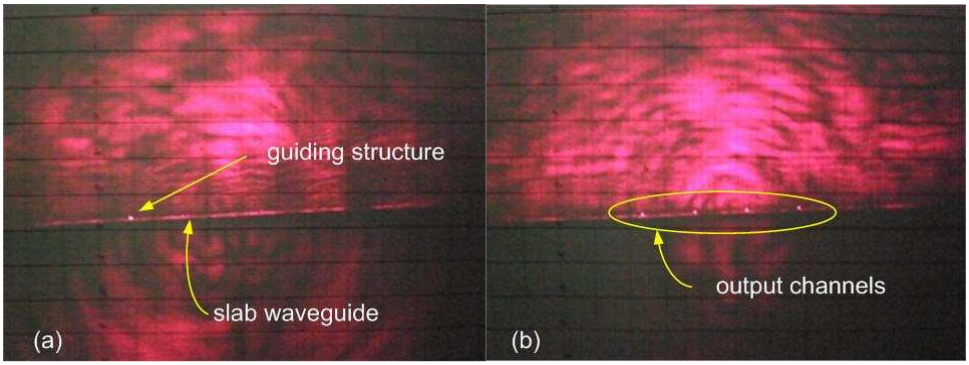

Fig. 5.6 (a) slab waveguide and guiding line structure structures; (b) four output channels from 1-by4 splitter

As the fiber continues to travel in downward direction, the twisted patterns disappear and replaced by an inverted interference pattern as shown in Fig 5.5c. Due to the platform for this planar optical device being a transparent material, the interference pattern is still clear to the naked eyes when the light source is at the bottom of waveguide. This situation will be harsh for eyes when an opaque material is used as the substrate. Fig.5.7 shows the UV written channel shows the result on the mentioned situation using planar device where the substrate is made of silicon wafer.

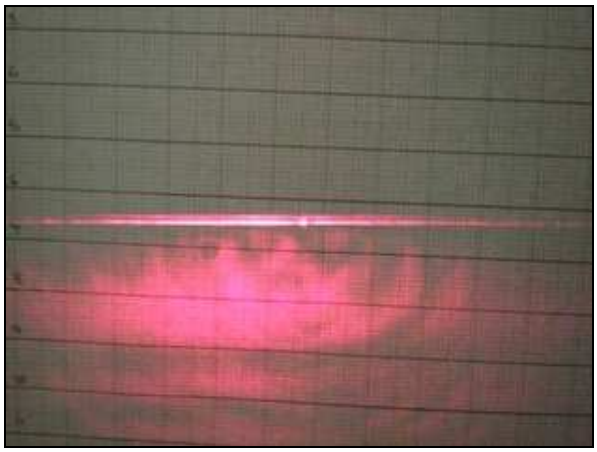

Fig. 5.7: UV-written single channel silica-on-silicon waveguide

5.1.3: Manual Alignment on Launch Fiber

After the input channel was located through the behavior of light at the medium with different refractive index; manual fine tuning on launch fiber position has been done to obtain an optimum output condition. Fig. 5.8 shows the optimum condition obtained from interference method.

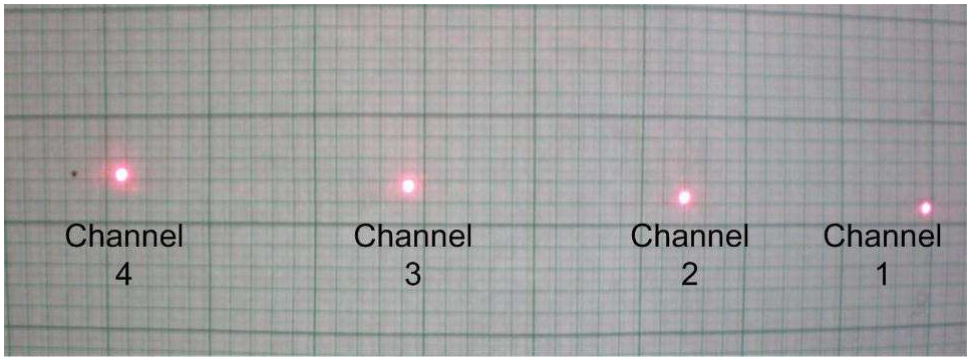

Fig. 5.8: Optimum condition achieved from manual alignment

Since a visible light source is utilized to provide information on input's location, the same optical signal is used in the manual alignment before it was replaced by optical signals in the wavelengths of 1310nm and 1550nm. However, the output was in multi-modal mode. Table 5.1 summarizes the coupling efficiency for each channel obtained from the manual alignment method on 1-by-4 optical power splitter coupled with signal at 650nm, and Fig. 5.9 reflects the insertion loss of each channels.

Table 5.1: Coupling efficiency of each channel from 1-by-4 optical power splitter

Channel	Coupling efficiency, η' (%)	Ideal coupling efficiency, η (%)
1	16.22	25.00
2	10.62	25.00
3	10.18	25.00
4	14.71	25.00

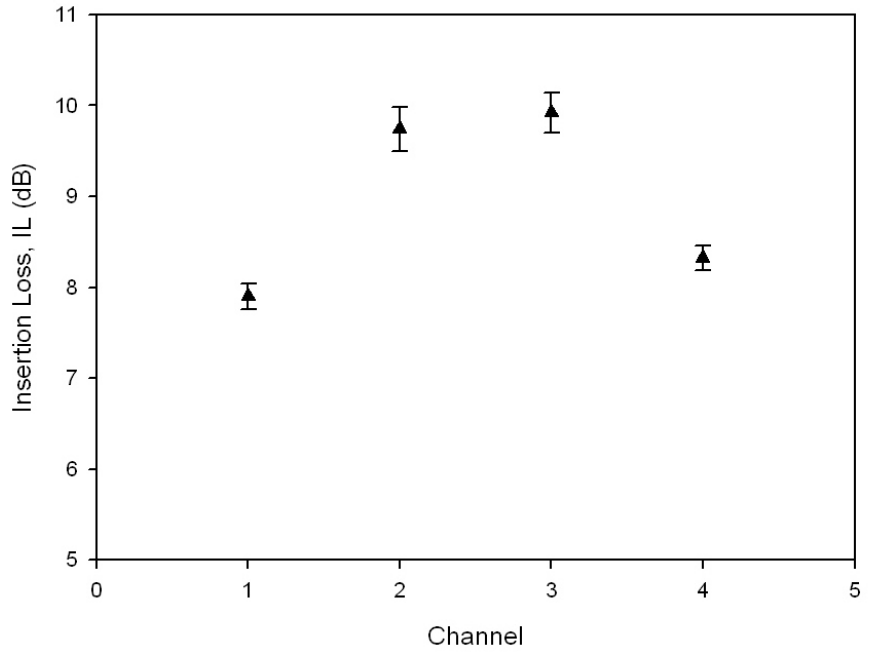

Fig. 5.9: Insertion loss of 1-by-4 optical power splitter coupled with signal at 650nm

Though the coupling efficiency obtained for each channel via manual alignment has large deviations from ideal, the insertion loss values are in the range of acceptance. The non persuaded coupling efficiency of each channel may be contributed by the imperfect surface quality on waveguide facets since the tested waveguide was only diced and not polished. The unpolished input facet scattered the incoming transmission signal even though index matching liquid was applied for fiber pigtailing. Again, the quality on transmission signal was disrupted by the same factor when leaving the output facet. In addition, scratches suffered by the end facet of fiber after few alignment attempts may reduce the transmission strength of optical signal too. However, the major contributor on the high insertion loss is due to the nature of the glass itself.

5.1.4: Peak Power Detection

After the manual alignment, a semi-automated peak power detection algorithm is used to refine the input channel location using transmission signal at 1310nm and 1550nm. Results on before and after the use of the algorithm for both the wavelengths are presented for comparison. Fig. 5.10 shows the insertion loss of the 1-by-4 optical power splitter coupled with optical signal at 1310nm, and Fig 5.11 shows the same measurement result using optical signal at 1550nm.

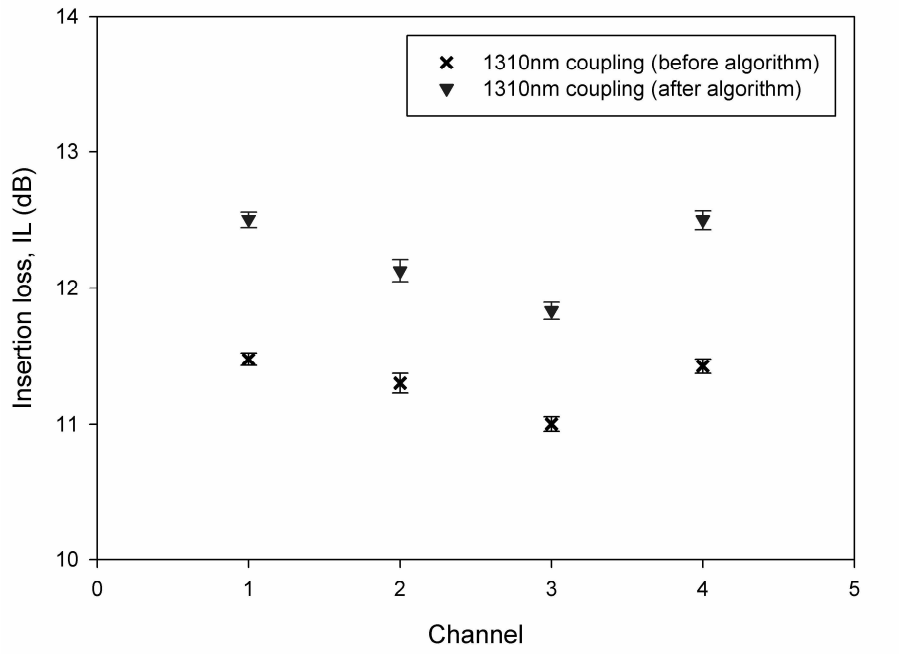

Fig. 5.10: Insertion loss of 1-by-4 optical power splitter coupled with optical signal at 1310nm

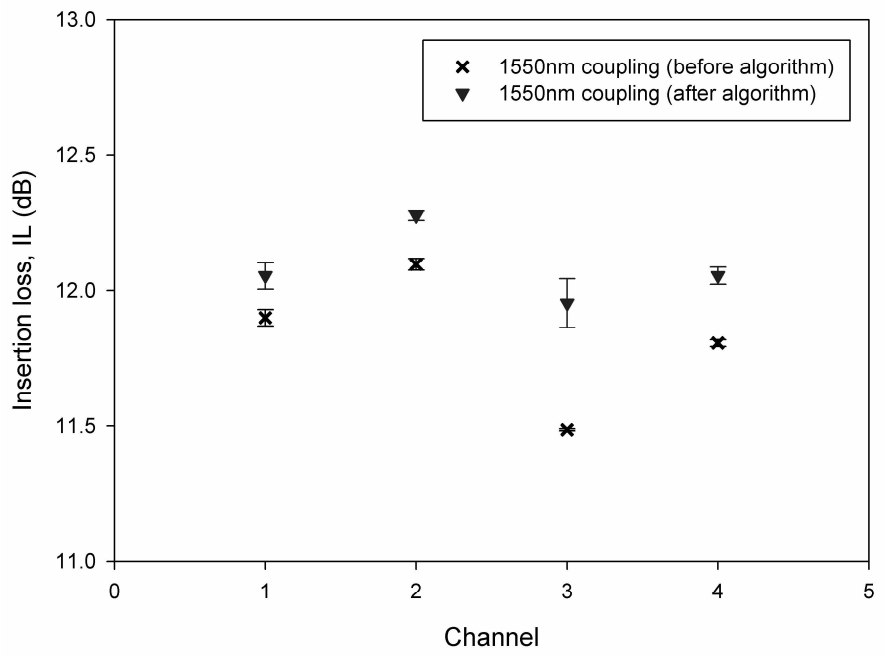

Fig. 5.11: Insertion loss of 1-by-4 optical power splitter coupled with optical signal at 1550nm

From Figs. 5.10 and 5.11, it is noticed that the insertion loss on the tested planar waveguide after the use of alignment algorithm was higher compared with result obtained from manual alignment. The reason for the algorithm inefficiency was thought to be related with the slow response from the computer where eventually creates an incorrect information feedback. This situation was occurred during the experiment. Instead of recording a reducing trend on transmitted power as the stage moves, the computer recorded a constant relationship between these two parameters (flat region in Fig. 4.5, Chapter 4). This situation still occurred when the algorithm was tested several times. For sure, such occurrence will miss out some important information especially on where the exact location of input channel is. As a possible solution to this setback, a time delay function may be included in the algorithm structure to synchronize all the command events. Besides, the backlash of the stepper motor itself was contribute to the inaccurate information on the input channel's position where this was observed under the simple vision system whereby the position of fiber was shifted after every stop of stepper motor stage.

It is also noticed from Fig. 5.9-Fig. 5.11, the trend of insertion loss is different for different wavelength. The inconsistent trend in the insertion loss may be caused by the shift on fiber's position after continuous alignment. Origins on the shifting were believed to be related to the backlash and positional repeatability of translational stage. Backlash is a sort of reaction exhibited by translational stage towards the intention of moving. This kind of repulsive action causes small deviations on the positional accuracy. Positional accuracy is about the ability of the translational stage to move back to the original position from where it began the movement. This situation is typical for any motor driven stage and is dependent on the type of motor used for movement control. For instance, servo motor driven stage has higher repeatability compared to stepper

motor driven stage. The other possible explanation on this situation may due to the operating region of the waveguide. The waveguide may be only optimized for wavelength at 1550nm. Hence the insertion loss trend will be different for different wavelengths.

From Fig. 5.9-Fig. 5.11, summary on the uniformity of the 1-by-4 optical power splitter is extracted and is shown by Table 5.2.

Table 5.2: Uniformity of 1-by-4 optical power splitter at different wavelength

Input wavelength, nm	**Uniformity, dB (before peak power detection)**	**Uniformity, dB (after peak power detection)**
650	2.021	-
1310	0.4711	0.6735
1550	0.6107	0.323

From the results shown in Table 5.2, peak power detection algorithm does not seems to undertake the assigned task well enough. However, the results are not able to reflect the whole situation. Fluctuations in uniformity may inherit from fabrication process, fiber displacement due to momentary movement of stepper, and perhaps the region of optical signal it optimized for.

5.2: UV Written Circuitries

This section presents the results obtained from the recent developed UV-writing coding. Due to some technical difficulties on glass fabrication in the lab, all the designed coding can be only transferred onto pieces of cards. Though the designs were not able to be transferred into in-house fabricated silica-on-silicon samples, some simple channels have been written on other materials. The samples are bulk silica made of 50% Bismuth (Bi) and of Germanium (Ge) fabricated by a PhD student from University Putra Malaysia (UPM), and in-house prepared Benzocyclobutene (BCB) polymer coated on silicon. Fig. 5.12 shows the written channel on the bulk silica sample, and Fig. 5.13 shows the straight channel written on BCB.

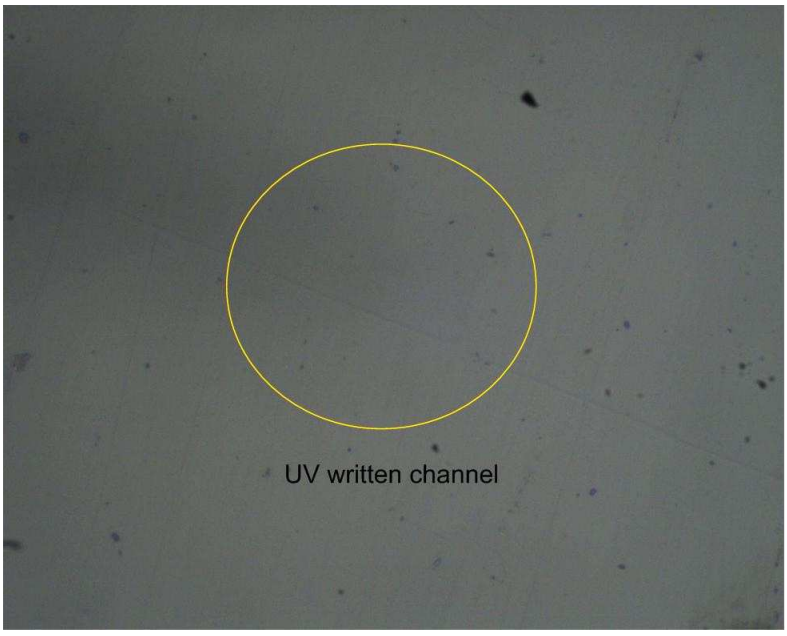

Fig. 5.12: UV written simple channel on bulk glass

Fig. 5.13: UV written straight channels on Benzocyclobutene (BCB) polymer

Circuitries for 1-by-2 optical power splitter and Mach Zehnder Interferometer (MZI) have been successfully written by the UV laser operated at 30mW with 3-axis motorized stage operated via LabVIEW platform. The processing parameters are presented in Table 5.3 below. The corresponding UV written optical circuitries are shown in Figs. 5.14 and 5.15.

Table 5.3: UV writing parameters of optical splitter and Mach Zehnder Interferometer

Parameter	**1-by-2 optical splitter**	**Mach Zehnder Interferometer**
Driving speed, (μm/s)	100	5000
Start up speed, (μm/s)	10	2500
Acceleration, (ms)	10	50
Dimension, length x width (μm)	12,000 x 200	17,000 x 1,000

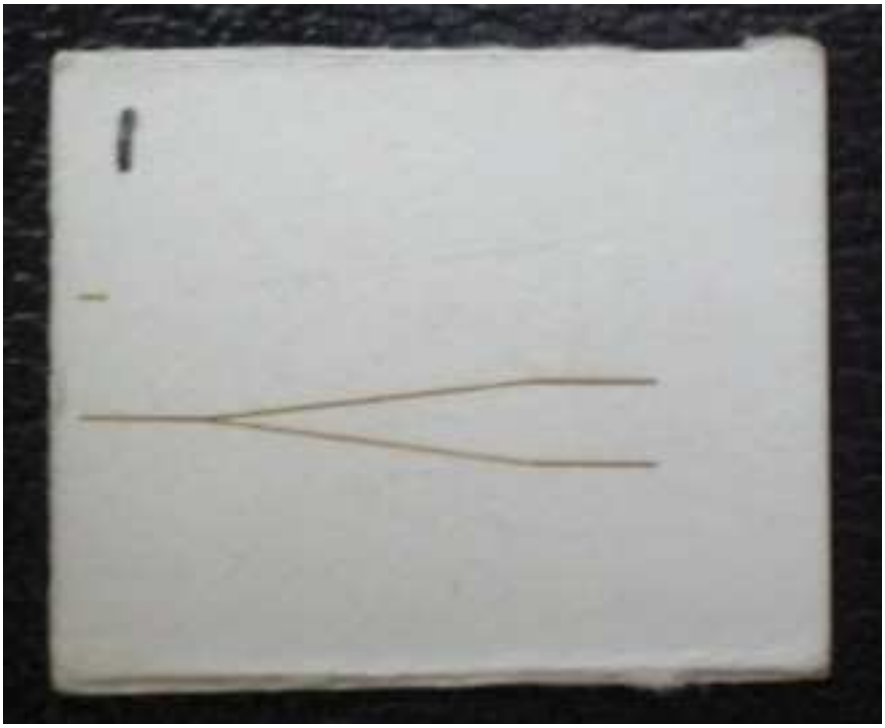

Fig.5.14: UV written 1-by-2 optical splitter circuit (transferred onto a card)

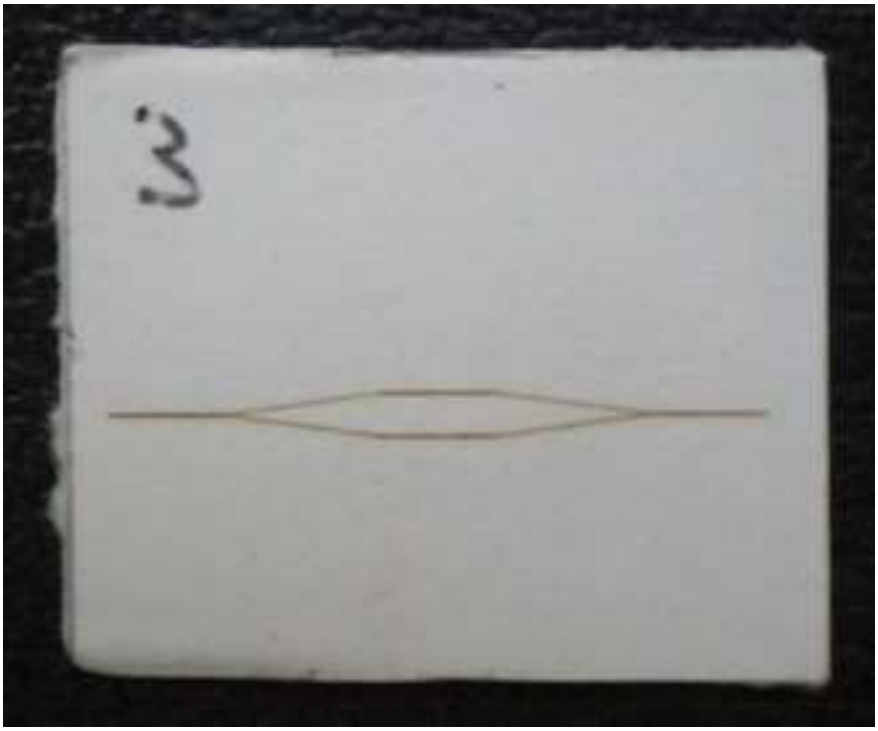

Fig. 5.15: UV written Mach Zehnder Interferometer circuit (transferred onto a card)

These UV writing coding architectures were not only tested in terms of their effectiveness in producing the desired circuitry, they were also in the aspect of time taken for circuit completion with respect to different driving speeds. Results on the time taken to complete circuit at different driving speeds are presented in Figs. 5.16 and 5.17. Throughout this testing, the start up speed and acceleration were maintained at 500μm/s and 10ms/s.

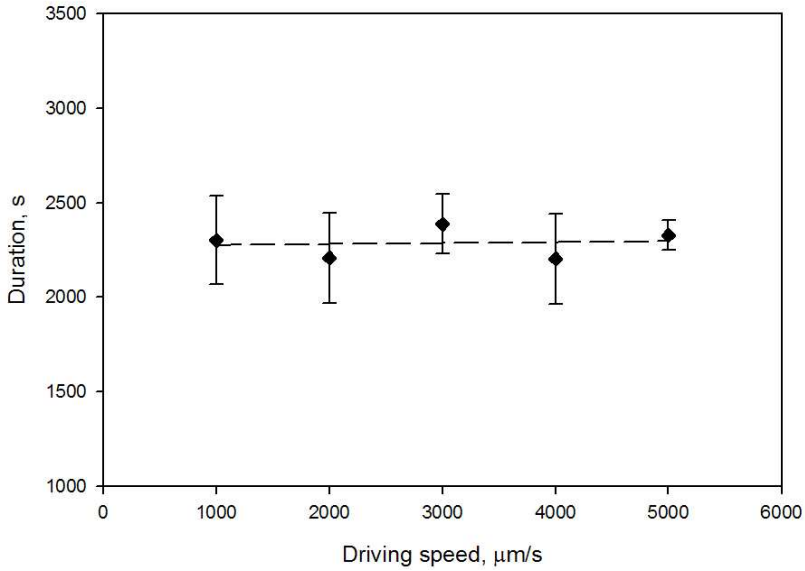

Fig. 5.16: Time taken to complete the design of 1-by-2 optical power splitter layout

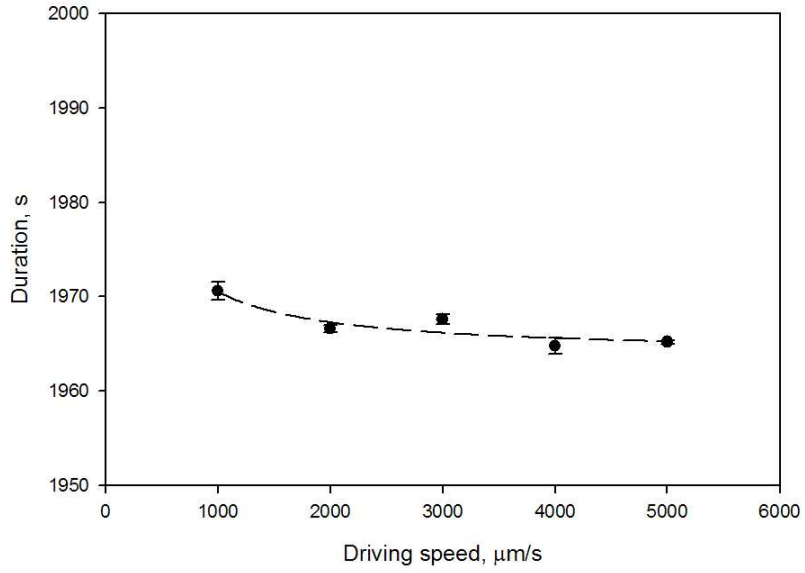

Fig. 5.17: Time taken to complete the design of Mach Zehnder Interferometer layout

Obviously, the time taken for circuit completion would depend on the dimension of the devices being fabricated, the driving speed and the complexity of the device architecture. From both Figs. 5.16 and 5.17, undoubtedly, both UV writing programs took quite some time to complete the circuit designs; where the average time taken to complete 1-by-2 optical power splitter design is about 38 minutes and the average to complete the design of Mach Zehnder Interferometer is about 32 minutes. Due to the long period and inconsistent in processing time, fundamental circuit designs: straight and slanted designs which using FOR loop in the coding development was analyzed. Results of the processing time of straight channel and slanted channel designs are presented in following figures: Figs. 5.18 and 5.19.

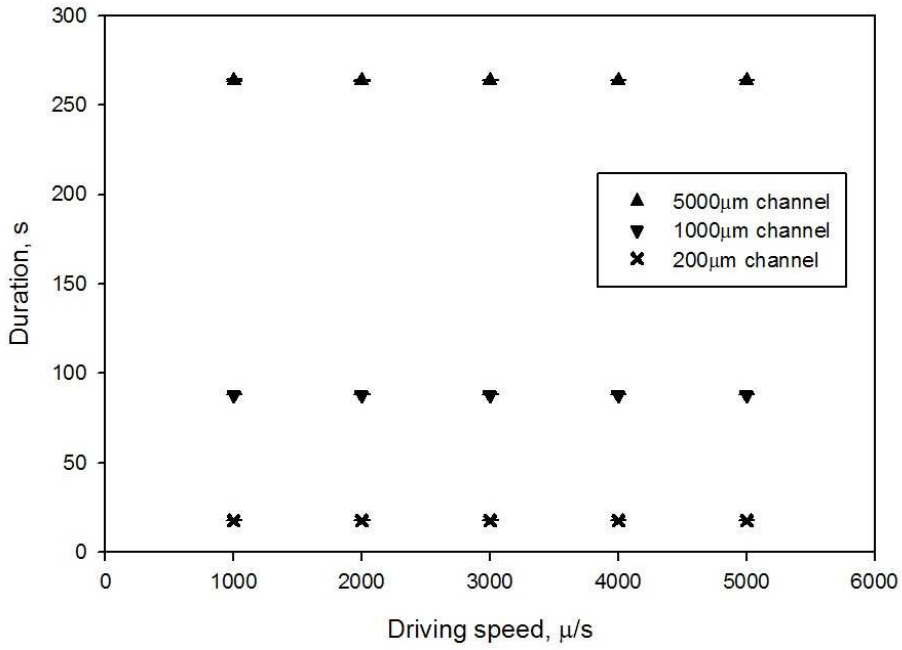

Fig. 5.18: Processing time for straight channel design at different channel lengths

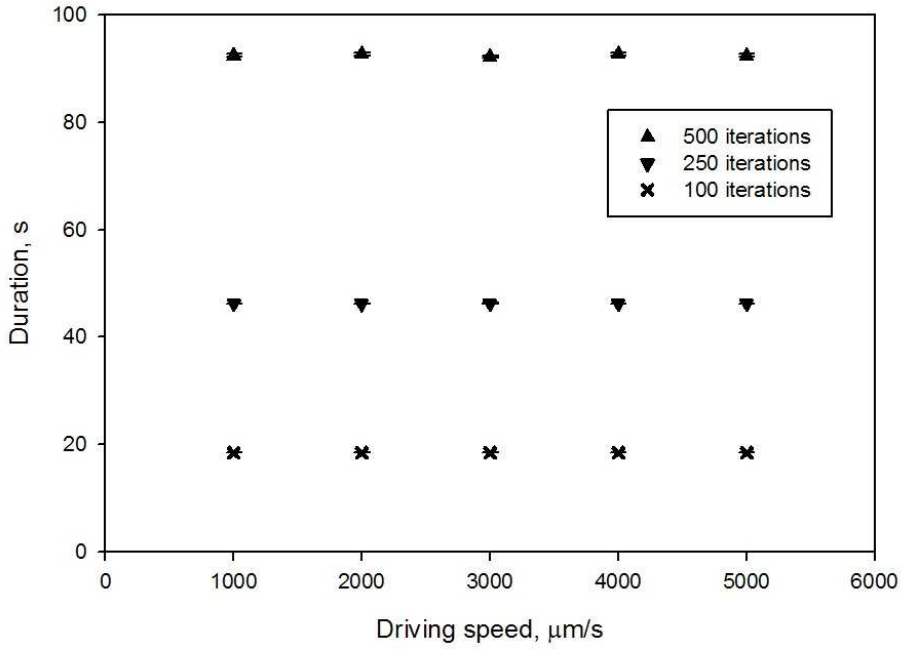

Fig. 5.19: Duration of time taken for slanted channel design at different iterations

From Figs. 5.18 and 5.19, time taken to complete both simple channel designs were consuming: about 18seconds is required to produce a 200µm length straight channel, and about 20 seconds is used to complete a 806.2µm length slanted channel yielded by 100 iterations of the coding structure. Since two circuitry designs were constructed from a series of collection on both the fundamental channel designs, therefore, it is time consuming in order to produce 1-by-2 splitter and Mach Zehnder Interferometer circuitries. The nearly constant relationship between driving speed and the duration of time shown in Figs. 5.16 and 5.17 is caused by the FOR loop command within the respective coding architectures. This type of command is processed at its own rate regardless of the commands on driving speed and is solely dependent on the number of instructions within the loop. In order to reduce the processing time, FOR loop which has been used in the coding architectures has been removed; results and coding of another straight channel coding structure is shown in Figs. 5.20 and 5.21 respectively.

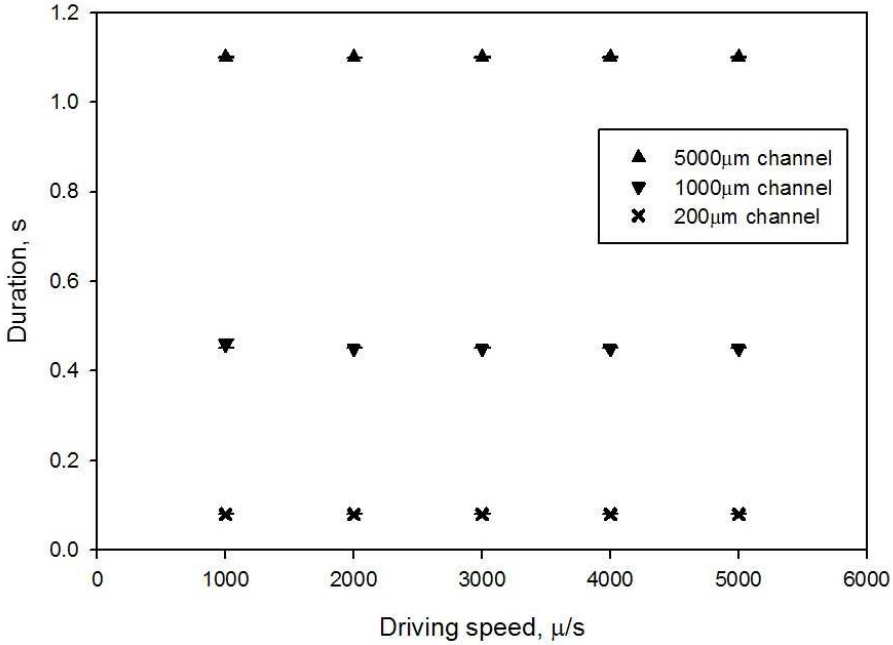

Fig. 5.20: Duration to complete straight channel in different length via coding architecture developed without using FOR loop

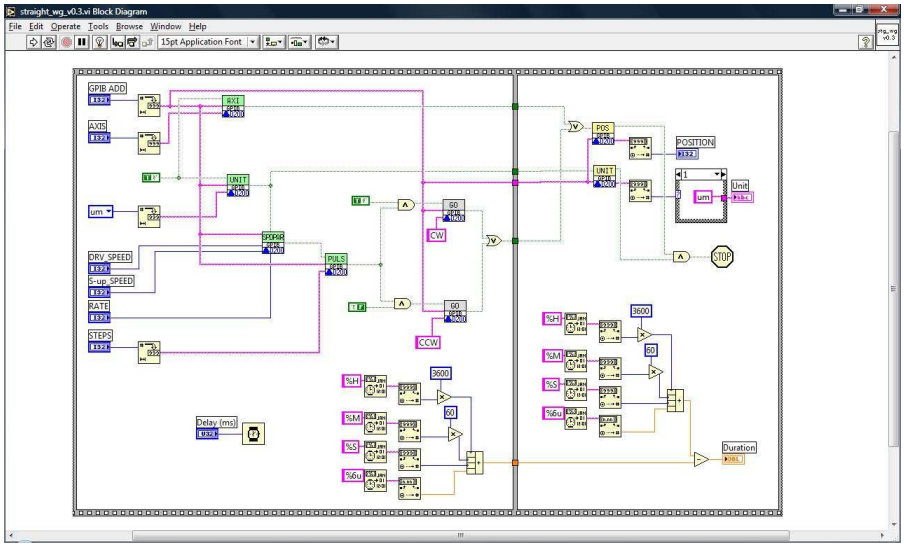

Fig. 5.21: Block diagram of straight channel writing coding architecture without the use of FOR loop

Apparently, from Fig. 5.18 to Fig. 5.20, FOR loop is responsible for the high processing time. When a coding architecture is developed without the use of the loop, the time to complete a similar circuit design has been reduced by 260%. The reason for FOR loop to be taking massive resources is due to the time needed to process the number of instructions within the iterative structure. This was obvious in this work where about 260 seconds were spent to process 40-over instructions by a FOR loop at 5000 iterations to complete 5000μm straight channel design at the speed of 1000μm/s. Under the same processing parameters, the coding developed without the use of FOR loop complete the channel design in about 1.1 seconds. However, as the flat relationship shown in Fig. 5.20, the coding was unable to deliver convincing result on how much time is require completing the coding at high driving speed. This is found to be related with the coding architecture where the design sends the whole coding commands to stepper motor for execution and stop running before the stop of stepper motor. Though a timer function was place within the architecture to synchronize the coding and stepper motor, it was not able to perform the task well. It is also found that parallel command processing is hardly occurred for a coding structure consisting two similar coding constructions. Parallel execution on two similar coding constructions causes a race between commands to be received and processed by stepper motor controller. As a result, only of them can be executed by the stepper motor. Therefore, coding architecture in Fig. 5.21 was not applied into the slanted circuit design since a slanted circuit design can only be realized sequential command structure.

5.3: Summary

In this work of optical planar waveguide alignment, numbers of alignment techniques have been developed according to few aspects: physical structure of waveguide and fiber, light interaction leaving planar waveguide to air, and the power transmitted from waveguide.

Though the simple vision system did not performed well in this work, it still appeared as an alternative for waveguide alignment. By eliminating the perspective error and identify the input channel's position, this vision method will sure works better. And having a high zoomed-in image at high resolution is going to reveal the coordinates precisely and therefore improve the alignment quality. Besides, with such precise information, image masking technique can be used as well.

Alignment technique developed from the interaction of light between materials with different index had demonstrated a positive throughput. This method was able to achieved insertion loss of about 11dB and 12dB when measured at the wavelength of 1310nm and 1550nm. Simplicity of this method has shortened the processing time in searching for the initial guiding light compared to the use of the power searching method. Later alignment technique is crucial in refining the input channel position. Hence, peak power detection alignment algorithm was therefore developed in this work. Sadly, this method failed to perform according to plan where it had jeopardized the low insertion loss vale obtained from interference based alignment method. Yet, the can be improved by synchronizing the processing events within the computing structure.

Despite the fact that circuitries for UV writing can be only transferred to pieces of card in this work, they have proved the concepts. The designed circuitries are: straight channel, slanted channel, 1-by-2 optical power splitter, and Mach Zehnder Interferometer. Success in the circuits transferred indicates the coding able to perform

the task effectively. Yet, they need to be transferred to the real platform, photosensitive glass, to test the functionality. Amendments on any of the UV writing coding architectures may be required in order to preserve the sensitivity nature of photosensitive sample during UV writing.

5.7: References

1. Optics and Optical Instruments Catalog, (Edmund Optics, 2008).